Heliyon 7 (2021) e07664

Contents lists available at ScienceDirect

Heliyon

journal homepage: www.cell.com/heliyon

Research article

Mineralogy and geochemistry of clay fractions in soils developed from different parent rocks in Limpopo Province, South Africa

O.O. Oyebanjo [a,*], G.E. Ekosse [b], J.O. Odiyo [a]

[a] School of Environmental Sciences, University of Venda, P/Bag X5050, Thohoyandou, 0950, South Africa
[b] Directorate of Research and Innovation, University of Venda, P/Bag X5050, Thohoyandou, 0950, South Africa

ARTICLE INFO

Keywords:
Soil kaolin
Mineralogy
Geochemistry
Crystallinity
Risk assessment

ABSTRACT

This study investigates the mineralogical and geochemical characteristics of clay fractions in soils developed from different parent rocks in Limpopo Province, South Africa using the X-ray diffraction (XRD), X-ray Fluorescence (XRF) Spectrometry, Laser Ablation – Inductively Coupled Plasma – Mass Spectrometry (LA-ICP-MS), Fourier Transform Infrared (FTIR) Spectrophotometry, Thermogravimetric Analysis and Differential Scanning Calorimetry (TGA-DSC) analytical techniques. Health risk associated with the presence of some trace elements was also investigated. The results revealed that the clay fractions had kaolinite as the dominant clay component occurring with other weatherable minerals. The crystallinity based on FTIR for the soil kaolinites correspond to partially - poorly ordered structures. The geochemical data showed appreciable accumulation of trace elements in the clay fractions. The absence of negative Ce anomaly in the chrondrite-normalised rare earth elements (REE) pattern in the clay fractions suggest the alteration of the primary minerals took place under suboxic conditions. The average non-carcinogenic hazard index (HI) were 1.52, 1.08, and 2.01 for children and 0.18, 0.13, and 0.24 for adults in the clay fractions from basalt, granite, and arkosic sandstone, respectively. The HI > 1 for children suggest non-carcinogenic health risk to children with ingestion pathway contributing the highest. The average carcinogenic risk index values were $>10^{-3}$ for children and adults with respect to Cr, Ni, and Pb in the clay fractions. This suggests very high carcinogenic risk to children and adult population in decreasing order from clay fractions in arkosic sandsone > basalt > granite, respectively.

1. Introduction

Kaolin minerals usually dominate the clay fractions of most weathered soil profiles in tropical and subtropical regions. The most common kaolin minerals occurring in soils are kaolinite followed by halloysite (Trakoonyingcharoen et al., 2006). Kaolin minerals in soils could be of primary origin through the weathering of rocks rich in aluminium or secondary in origin through the weathering of arkosic rocks (Ekosse, 2005).

The most popular of all South African soils is the Hutton form, which accounts for the marvelous redness of the landscape across the Country. According to Mzezewa et al. (2010), the Hutton form soil type in the study areas is similar to Rhodic Eutrustox (Soil Survey Staff, 2006) or Rhodic Ferralsol (WRB, 2006). The apedal (structureless) soils in the group are characterised by a relatively low CEC (<11 $cmol_c$ kg^{-1}) reflecting oxidic mineralogy with predominantly kaolinitic assemblage (Fey, 2010). The geochemical and mineralogical composition of the clay fraction has significant implications on soil fertility, geochemical exploration and engineering properties (Schaefer et al., 2008). Trace elements in soil clay fractions are important in health risk assessment because of their ability to accumulate higher amounts relative to the bulk soil (Luo et al., 2011). The elements can leach into groundwater or end up in the food chain through plant uptake (Acosta et al., 2009). Hence, the fraction in which trace elements are more accumulated would pose the most serious health threat (Kicinska, 2018).

Despite the dominance of kaolin in these soils, little is known of their properties in the medium (Yoothong et al., 1997). Previous researches conducted in South Africa on kaolins are limited to standard kaolins with little or no publication on soil kaolin leading to a great omission in the overall clay minerals body of knowledge. The study of pure or standard clay deposit may serve as a basis in understanding kaolin in soils. Hart et al. (2002) and Hughes et al. (2009) reported that soil kaolin characteristics differ greatly when compared to standard mineral kaolin in that the former typically have high defect structures, complex crystal

* Corresponding author.
E-mail address: omosalewadewale@gmail.com (O.O. Oyebanjo).

https://doi.org/10.1016/j.heliyon.2021.e07664
Received 20 May 2020; Received in revised form 17 January 2021; Accepted 22 July 2021

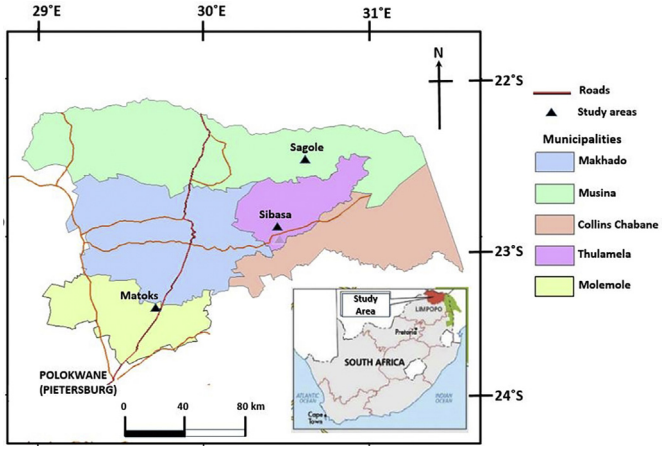

Figure 1. Map of Limpopo Province showing the locations of the study areas (Modified after Hall et al., 2013).

morphologies, smaller crystal size, and significant structural iron. Based on studies on soil kaolins from Indonesia, Western Australia, and Thailand, Hart et al. (2002, 2003) observed significant differences in their properties within a single geographic region and particularly within a single profile. Therefore, this study is directed towards unraveling the variations in the clay mineralogical and geochemical characteristics in soils developed from different parent rocks (basalt, granite, and arkosic sandstone) in Limpopo Province, South Africa. Several studies have reported health implications associated with trace elements in clay fractions to plants (e.g Kabata-Pendias, 2011; Luo et al., 2011; Gomes et al., 2016). The risk assessment based on some trace elements present in the clay fractions (0–20 cm) was also investigated.

2. Location and geological setting

The studied soil profiles developed from basalt, arkosic sandstone, and granite are in Sibasa (Thulamela Municipality), Sagole (Musina Municipality), Matoks (Molemole Municipality) areas, respectively, Limpopo Province, South Africa (Figure 1).

The soil profiles developed from basalt and arkosic sandstone occur within the Sibasa Basalt Formation and Wyllie's Poort Formation respectively of the Soutpansberg Group (Figure 2a). The stratigraphy of the Group comprises of both volcanic and sedimentary succession which has been subdivided into six formations namely: Nzhelele, Musekwa, Wyllie's Poort, Fundudzi, Sibasa, and Tshifhefhe, respectively (SACS, 1980; Brandl, 1999 and Barker et al., 2006).

The Sibasa Basalt Formation is a sequence composed of cyclically erupted basalts. They are generally aphanitic – fine grained with colour variation from blackish to light green depending on the degree of epidotisation. Amygdaloidal varieties have vesicles filled with quartz and chalcedony. The matrix is made up of clinopyroxene (mainly augite) and plagioclase. Interbedded clastic sediments which include quartzite, shale, and minor conglomerate locally reach a maximum of 400 m. The formation thickness is estimated to reach about 3000 m (Barker et al., 2006).

The Wyllie's Poort Formation according to Brandl (1981) underlies the major part of the more mountainous ground of the Soutpansberg Group. Its basal contact has been interpreted as a regional unconformity (Cheney et al., 1990). It is medium-to coarse grained with prominent agate conglomerate at the base in some areas. Towards the eastern part of Tshipise, the uppermost portion of the formation is well-bedded, light coloured feldspathic (arkosic) sandstone. In addition, minor lenticular intercalations of basaltic lava and pyroclastic rocks are developed in the eastern regions. Its maximum recorded thickness is 1,500 m.

The soil profiles developed from granite occur within the Matok Granite Suite of the Southern Marginal Zone, Limpopo Belt (Figure 2b). The Matok Granite is emplaced north of the Hout River Shear zone. It intruded an earlier charno-enderbitic unit which occurs preferentially in the northern part of the granite body. The granite is whitish to pink in colour, medium grained to porphyritic with a range of composition from granitic to granodioritic while the charnockitic suite comprises of both enderbite and charno-enderbite. The charno-enderbitic units are fine-to medium grained, greyish green to olive green rocks that are composed of quartz, plagioclase, orthoclase, hyperstene, and augite. Radiometric ages between 2663 and 2666 Ma from zircon U–Pb dating have been recorded for the granitic suite (Barton et al., 1992).

3. Materials and methods

Soil profiles developed from basalt, granite, and arkosic sandstone, respectively were sampled at depths ranging from 0 - 20, 20–50, and 50–100 cm depending on where the hard rock begins using a soil auger. Information on the geology, coordinates, soil types, profile description, climate, and number of samples are presented in Table 1a. Disaggregated (by gentle crushing) and air-dried samples were dispersed with Calgon (Sodium hexametaphosphate and Soda) (Van Reeuwijk, 2002) and

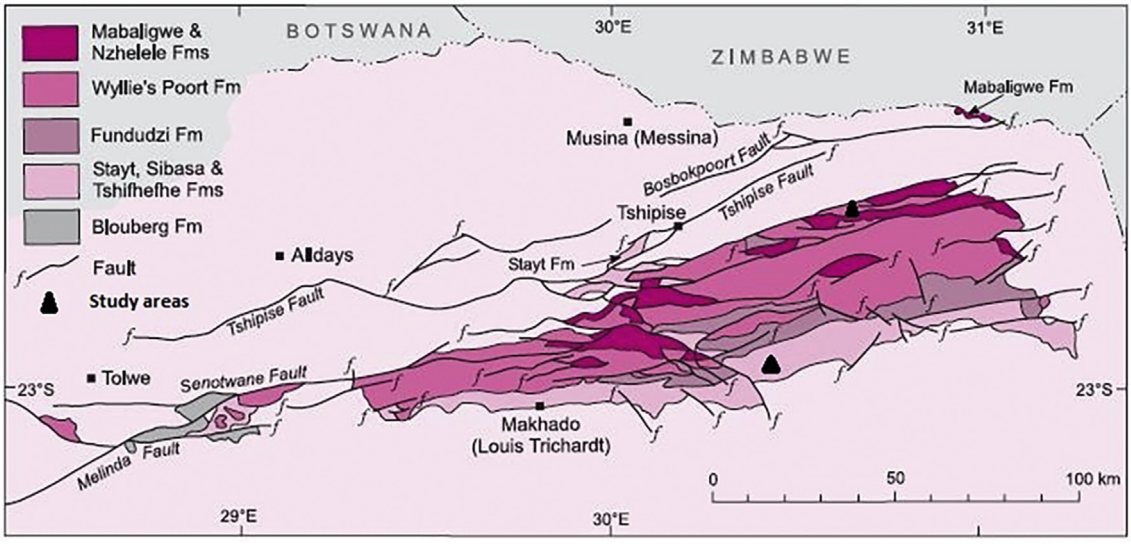

Figure 2a. Geologic Map of the Soutpansberg Group showing the study areas (Modified after Barker et al., 2006).

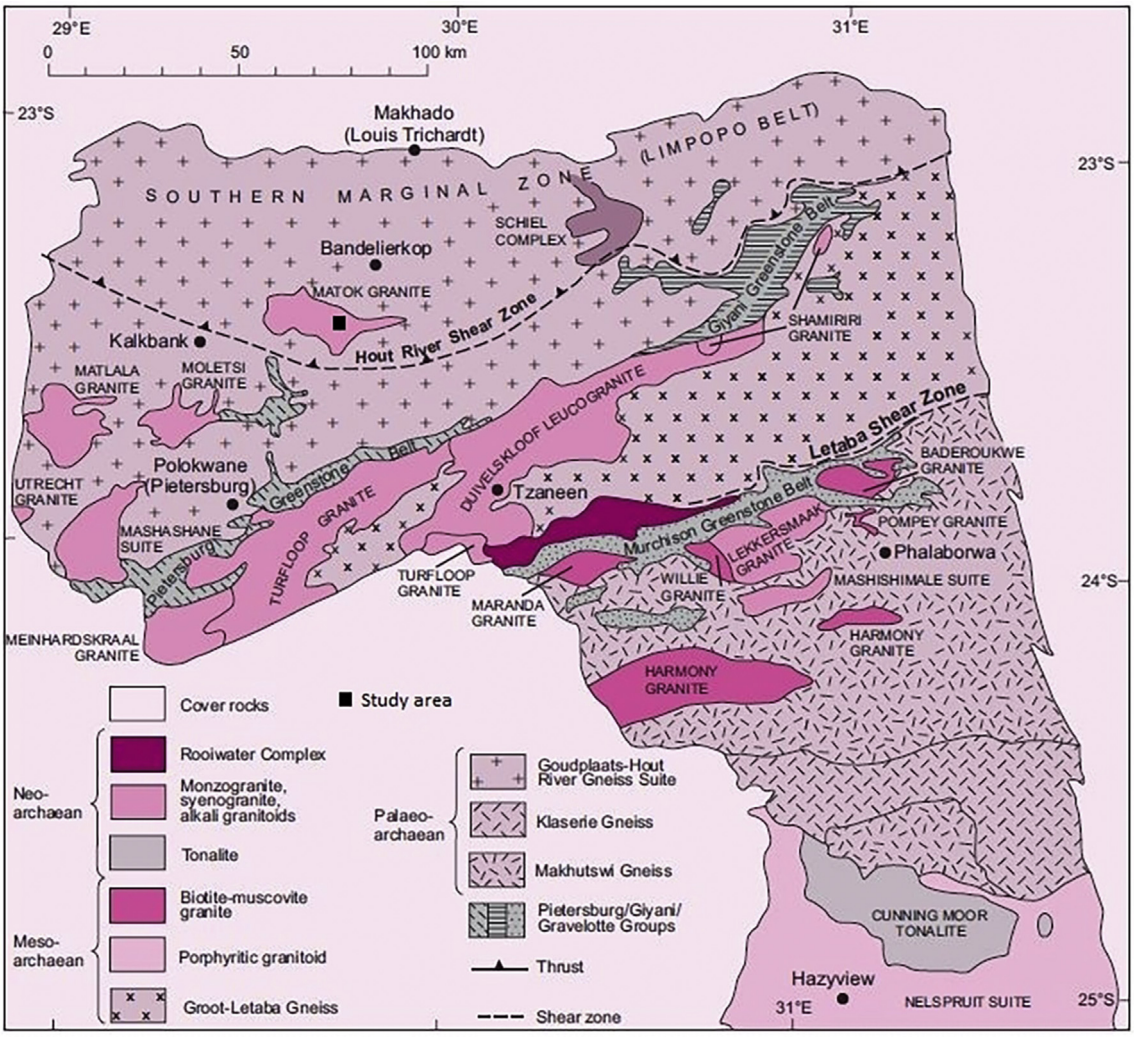

Figure 2b. Geologic Map of the Southern Marginal Zone (Limpopo Belt) and Northern Sector of the Kaapvaal Craton showing the study area (Modified after Robb et al., 2006).

ultrasonic disintegrator as described by Suslick and Price (1999), Jakubowska (2007), and Raty and Peltovuori (2008) to obtain the clay fractions (<2 μm). The ultrasonication was done with an energy input of 300 J m/L (1 min) using probe type ultrasonic disintegrator UP400S equipped with 7 mm diameter sonotrode S7 at the Department of Ecology and Resource Management, University of Venda (UNIVEN), South Africa.

The clay fractions were analysed using a PANalytical X'Pert Pro powder X-ray diffractometer with an X'Celerator detector and variable divergence- and fixed receiving slits with Fe filtered Co-Kα radiation ($\lambda = 1.789$ Å). Samples were scanned from 2° 2θ to 85° 2θ at a counting time of 0.5 s. The X'Pert Highscore plus software was used for phase identifications and the Rietveld method was used to compute their relative percentages with an accuracy within approximately ±3 wt % as described by Hillier (2000). The peaks at 14 Å and 7 Å could also be attributed to clay minerals such as chlorite, vermiculite and/or smectite, which would require further analysis to confirm the mineral species.

Table 1a. Information on the study areas and number of samples (Adapted from Oyebanjo, 2020).

S/N	Lithology/Location	Coordinates	Soil Type		Profile Description	Climate	Number of samples
			Form	Series			
1.	Basalt/Sibasa	S1 - 22° 57' 09" S 30° 27' 10" E S2 - 22° 57' 27" S 30° 27' 51" E	Hutton	Portsmouth (35)	Orthic A with deep red apedal B horizon	Semi-Arid, dry hot (BSh)	6 (0–20, 20–50, 50–100 cm)
2.	Granite/Matoks	MAT1 - 23° 27' 46" S 29° 44' 03" E MAT2 - 23° 27' 16" S 29° 44' 48" E	Hutton	Portsmouth (35)	Orthic A with shallow yellow-brown apedal B horizon	Warm temperate, winter dry, hot summer (CWa)	4 (0–20, 20–50 cm)
4.	Arkosic Sandstone/Sagole	SA1 - 22° 31' 01" S 30° 36' 54" E SA2 - 22° 30' 20" S 30° 36' 44" E	Hutton	Portsmouth (35)	Orthic A with shallow yellow-brown apedal B horizon	Semi-Arid, dry hot (BSh)	3 (0–20, 20–50 cm)

Table 1b. Description of parameters and values used in Equations 2–6 (Adapted from Qing et al., 2015; Weissmannova et al., 2019 and references therein).

Parameters	Description	Values
C (mg kg^{-1})	Element content in soil	
CF (kg mg^{-1})	Conversion factor	10^{-6}
EF (day yr^{-1})	Exposure frequency	350
ED (yr)	Exposure duration	6 and 30 for children and adults, respectively
BW (kg)	Body weight	16 and 70 for children and adults, respectively
AT_{nc} (day)	Average time for non-carcinogenic effects	2190 and 10950 for children and adults, respectively
AT_{ca} (day)	Average time for carcinogenic effects	25550
Ingestion		
Ing*R* (mg day^{-1})	Ingestion rate	200 and 100 for children and adults, respectively
Inhalation		
Inh*R* (m^3 day^{-1})	Respiratory rate	20
PEF (m^3 kg^{-1})	Particulate emission factor	1.39×10^9
Dermal contact		
SA (cm^2)	Skin Surface Area	2800 and 5700 for children and adults, respectively
AF (mg cm^{-2} day^{-1})	Adherence factor	0.2 and 0.07 for children and adults, respectively
ABS (Unitless)	Absorption factor	0.001 for all metals

	Cr	Ni	Zn	Pb	Cu	Co
RfD_{ing} (mg kg day^{-1})	3.00×10^{-3}	0.02	0.3	3.50×10^{-3}	0.04	0.02
RfD_{inh} (mg kg day^{-1})	2.86×10^{-5}	9.00×10^{-5}	0.3	3.52×10^{-3}	0.04	-
RfD_{derm} (mg kg day^{-1})	6.00×10^{-5}	5.40×10^{-3}	0.06	5.25×10^{-4}	0.12	-
SF for ingestion (kg day mg^{-1})	0.5	-	-	8.50×10^{-3}	-	-
SF for inhalation (kg day mg^{-1})	42	0.84	-	-	-	-

RfD – reference dose; SF – slope factor, (-) not available.

The infrared spectra (IR from 400 to 4000 cm^{-1} with a resolution of 4 cm^{-1}) were obtained for the kaolin in the clay fractions using a Bruker Alpha Platinum – Attenuated total reflectance (ATR) Spectrometer at the Department of Ecology and Resource Management, UNIVEN, South Africa following the procedures outlined by Madejova and Komadel (2001). A TA instrument SDT Q600 TGA-DSC analyser at the Department of Chemistry, University of Johannesburg (UJ) was used to determine the thermogravimetric property of the kaolin. The sample (10 mg) was heated from 25 to 1100 °C at 10 ℃/min.

For the major element compositions of the clay fractions, glass disks were prepared for X-ray fluorescence (XRF) and measured on a PANalytical Axios Wavelength Dispersive spectrometer fitted with a Rh tube. Reference standards were ran for calibration procedures. The Loss on Ignition (LOI) was determined following the procedures described by Van Reeuwijk (2002).

A Resolution 193 nm Excimer laser from ASI connected to an Agilent 7700 Inductively Coupled Plasma – Mass Spectrometry (ICP-MS) was used in the analysis of trace elements in the clay fractions. The samples were ablated using a frequency of 10 Hz and 2 mJ energy in helium gas at 0.35 L/min mixed with argon (0.9 L/min) and nitrogen (0.004 L/min) before measurement (Gunther and Hattendorf, 2005). Reference standards were ran for calibration procedures. The geochemical analyses were carried out at the Central of Analytical Facilities, University of Stellenbosch, South Africa.

To assess the enrichment of some trace elements in the clay fractions reported in this study such as Cr, Ni, Zn, Pb, Co, and Cu considered to be

Table 2. Results of quantitative analyses of minerals present (wt %) in the clay fractions developed from different parent rocks.

Parent rock	Sample ID	Kao	Qtz	Anatase	Goe	Hem	Plag	Mic	Mus/Ill	Gibbsite	Chlorite	Actinolite
Basalt	S1 0–20 cm	62	22	8	-	8	-	-	-	-	-	-
	S1 20–50 cm	64	18	7	4	7	-	-	-	-	-	-
	S1 50–100 cm	82	8	2	5	-	-	-	-	3	-	-
	S2 0–20 cm	77	10	3	5	4	-	-	-	1	-	-
	S2 20–50 cm	85	7	2	5	-	-	-	-	1	-	-
	S2 50–100 cm	77	9	3	6	4	-	-	-	1	-	-
	Average	74.50	12.33	4.17	5	5.75	-	-	-	1.50	-	-
Granite	MAT1 0–20 cm	31	21	-	-	-	20	10	17	-	-	1
	MAT1 20–50 cm	24	20	-	-	-	24	14	14	-	2	2
	MAT2 0–20 cm	26	19	-	-	-	32	9	13	-	-	1
	MAT2 20–50 cm	29	20	-	-	-	22	9	14	-	4	2
	Average	27.50	20	-	-	-	24.50	10.50	14.50	-	3	1.50
Ark. Sst	SA1 0–20 cm	23	35	-	-	-	-	17	25	-	-	-
	SA2 0–20 cm	26	27	-	-	-	-	19	24	-	5	-
	SA2 20–50 cm	24	38	-	-	-	-	13	19	-	6	-
	Average	24.33	33.33	-	-	-	-	16.30	22.66	-	5.50	-

Kao – kaolinite; Qtz – quartz; Goe – goethite; Hem – hematite; Plag – plagioclase; Mic – microcline; Mus – muscovite; Ill - illite.

Table 3a. IR band positions and assignments of soil kaolinites developed from different parent rocks and theoretical kaolinite.

Theoretical Kaolinite	Basalt	Granite	Arkosic Sandstone	Assignment
3691–89	3692	3683	3684	Al- - -O–H stretching of inner surface hydroxyl groups
3669	-	3669–3663	3670	Al- - -O–H stretching of inner surface hydroxyl groups
3651	-	3647–3641	-	Al- - -O–H stretching of inner surface hydroxyl groups
3619	3620	3620	3620	Al- - -O–H stretching of inner hydroxyl groups
1115–14	1114	1107	1114	Si–O stretching (Longitudinal mode)
1028–27	1043	1037–1024	1025	In-plane Si–O stretching
1005–04	1007–998	1000	998	In-plane Si–O stretching
937–935	-	936–935	936	OH deformation of inner surface hydroxyl groups
912	910–903	907–905	913	OH deformation of inner hydroxyl groups
789–788	-	791	793	OH deformation linked to Al, Mg
751–750	-	749	743	Si–O perpendicular
541	-	525	525	Fe–O, Fe_2O_3, Ti–O; Si–O–Al stretching

Note: MAT2 20–50, SA2 0–20, and SA2 20–50 do not have IR kaolinite bands.

of most interest in South African context (Herselman, 2007), the accumulation factor (AF) was calculated using the relationship as expressed in Eq. (1) (Ajmone-Marsan et al., 2008).

$$AF = X_{cf}/X_{bulk} \quad (1)$$

where, X_{cf} and X_{bulk} are the concentrations (ppm) of the trace element in the clay fraction and the bulk soil, respectively. The trace element concentrations in the bulk soils have been earlier reported (Oyebanjo et al., 2020). Trace elements with AF > 1 suggests that it is accumulated in the clay fraction (Acosta et al., 2009).

The AF does not reflect the level of health risk to human. The non-carcinogenic hazard index (HI) and carcinogenic risk index (CRI) were used to assess the health risk associated with the trace elements present in the clay fractions (topsoils, 0–20 cm) since they are preferential enriched in them. The HI and CRI through the different routes were computed using Equations 2–6 (Luo et al., 2012; Gao et al., 2019; Kumar et al., 2019). The definition of parameters and values used in equations are listed in Table 1b.

$$HI = \sum_{i=1}^{n} HQ = \sum_{i=1}^{n} \left(\frac{ADI^{i}_{ing}}{RfD^{i}_{ing}}\right) + \sum_{i=1}^{n} \left(\frac{ADI^{i}_{inh}}{RfD^{i}_{inh}}\right) + \sum_{i=1}^{n} \left(\frac{ADI^{i}_{derm}}{RfD^{i}_{derm}}\right) \quad (2)$$

$$\begin{aligned} CRI &= \sum_{i=1}^{n} \left(CRI^{i}_{ing} + CRI^{i}_{inh} + CRI^{i}_{derm}\right) \\ &= \sum_{i=1}^{n} \left(ADI^{i}_{ing} \times SF^{i}_{ing}\right) + \sum_{i=1}^{n} \left(ADI^{i}_{inh} \times SF^{i}_{inh}\right) \\ &\quad + \sum_{i=1}^{n} \left(ADI^{i}_{derm} \times SF^{i}_{derm}\right) \end{aligned} \quad (3)$$

$$ADI_{ing} = \frac{C \times IngR \times EF \times ED \times CF}{BW \times AT} \quad (4)$$

Table 3b. Structural order and dehydroxylation temperatures of kaolinites in soils developed from different parent rocks using IR-N classification.

Parent Rock	Sample ID	$I(V_1)$	$I(V_3)$	$I(V_4)$	CI_1	CI_2	Degree of Crystallinity	Dehydroxylation Temperature (C)
Basalt	S1 0–20 cm	0.92	0.93	0.92	0.99	1.00	Pao	457
	S1 20–50 cm	0.94	0.93	0.94	1.00	1.00	Pao	467
	S1 50–100 cm	0.84	0.82	0.84	1.01	1.00	Pao	475
	S2 0–20 cm	0.92	0.93	0.92	0.99	1.00	Pao	467
	S2 20–50 cm	0.95	0.87	0.95	1.09	0.99	Pao	467
	S2 50–100 cm	1.04	0.89	1.05	1.17	1.00	Pao	475
	Min				0.99	0.99		457
	Max				1.17	1.00		475
	Average				1.04	1.00	Pao	468
Granite	MAT1 0–20 cm	0.92	0.70	0.92	1.32	1.00	Pao	467
	MAT1 20–50 cm	1.08	0.96	1.07	1.13	0.99	Pao	430
	MAT2 0–20 cm	0.97	0.81	0.96	1.20	1.00	Pao	430
	MAT2 20–50 cm	0.95	0.96	0.95	0.99	1.00	Pao	425
	Min				0.99	0.99		425
	Max				1.32	1.00		467
	Average				1.16	1.00	Pao	438
Arkosic Sandstone	SA1 0–20 cm	0.97	0.81	0.97	1.20	1.00	Pao	
	SA2 0–20 cm	0.87	0.91	0.89	0.95	1.01	Pao	
	SA2 20–50 cm	0.92	0.94	0.93	0.98	1.01	Pao	
	Min				0.95	1.00		
	Max				1.20	1.01		
	Average				1.04	1.01	Pao	

$I(v_1)$, $I(v_3)$, and $I(v_4)$ are intensities at 3691/3689 cm^{-1}, 912 cm^{-1}, and 3619 cm^{-1}; $CI_1 = I(v_1)/I(v_3)$ and $CI_2 = I(v_4)/I(v_1)$; (pa-o): Partially ordered ($0.7 < CI_1 < 0.8$ and $0.9 < CI_2 < 1.2$) Vaculikova et al. (2011) and references therein).

Table 4. Major element oxides (wt %) of clay fractions in soils developed from different parent rocks in Limpopo Province, South Africa and for average Thailand Oxisols (basalt) and Ultisols (granite).

Parent Rock	Sample ID	SiO_2	TiO_2	Al_2O_3	Cr_2O_3	Fe_2O_3	CaO	MgO	MnO	K_2O	Na_2O	P_2O_5	L.O.I.	SiO_2/Al_2O_3
Basalt	S1 0–20 cm	37.06	2.38	23.69	0.03	17.86	0.10	0.18	0.09	0.33	1.69	0.15	16.70	1.56
	S1 20–50 cm	37.12	2.21	24.99	0.02	16.50	0.06	0.18	0.07	0.39	1.97	0.13	16.28	1.49
	S1 50–100 cm	32.74	2.82	25.09	0.03	20.50	0.04	0.03	0.08	0.05	1.69	0.14	17.30	1.30
	S2 0–20 cm	36.85	2.12	23.18	0.05	17.19	0.11	0.17	0.06	0.20	2.09	0.16	17.85	1.59
	S2 20–50 cm	34.01	2.05	23.57	0.06	18.19	0.10	0.15	0.06	0.17	2.15	0.13	19.53	1.44
	S2 50–100 cm	39.51	1.90	24.54	0.03	14.68	0.04	0.13	0.06	0.08	2.10	0.11	16.86	1.61
	Average	36.22	2.25	24.18	0.04	17.49	0.08	0.14	0.07	0.20	1.95	0.14	17.42	1.50
Granite	MAT1 0–20 cm	64.97	1.27	16.33	0.01	2.64	1.53	0.91	0.05	2.40	4.38	0.08	4.70	3.98
	MAT1 20–50 cm	62.17	1.25	16.25	0.01	2.85	1.31	0.85	0.05	2.28	4.94	0.08	6.96	3.83
	MAT2 0–20 cm	63.89	1.36	15.83	0.01	3.40	1.71	1.32	0.05	2.44	4.40	0.13	4.93	4.04
	MAT2 20–50 cm	65.91	1.40	15.80	0.01	2.81	1.70	1.16	0.06	2.57	4.46	0.08	3.80	4.17
	Average	64.24	1.32	16.05	0.01	2.93	1.56	1.06	0.05	2.42	4.55	0.09	5.10	4.00
Ark. Sandstone	SA1 0–20 cm	66.73	2.68	12.51	0.06	3.42	0.39	0.46	0.03	4.57	2.06	0.07	6.18	5.33
	SA2 0–20 cm	56.43	2.17	14.94	0.05	4.42	0.81	1.17	0.04	3.95	2.11	0.27	13.45	3.78
	SA2 20–50 cm	55.18	2.13	15.46	0.05	4.45	0.77	1.20	0.04	4.02	2.72	0.26	13.15	3.57
	Average	59.45	2.33	14.30	0.05	4.10	0.66	0.94	0.04	4.18	2.30	0.20	10.93	4.16
Thailand Oxisols[1]	Average	28.45	3.84	27.96	-	19.30	0.14	0.33	0.26	0.12	-	1.88	-	1.02
Thailand Ultisols[1]	Average	43.21	0.83	35.14	-	4.15	0.14	0.17	0.01	0.36	-	1.60	-	1.23

[1] Darunsontaya et al. (2010) and bdl = below detection limit.

$$ADI_{inh} = \frac{C \times InhR \times EF \times ED}{PEF \times BW \times AT} \quad (5)$$

$$ADI_{derm} = \frac{C \times SA \times AF \times ABS \times EF \times ED \times CF}{BW \times AT} \quad (6)$$

4. Results and discussion

4.1. Mineralogical characteristics

The percentages of the various minerals present in the clay fractions are presented in Table 2. The clay fractions in soils developed from basalt were mainly composed of kaolinite, quartz, anatase, goethite, hematite, and gibbsite. Kaolinite and quartz were the dominant components ranging from 82 to 92 wt % with >60 wt % kaolinite. The non-clay minerals constituted <18 wt % in all the samples with Ti-bearing mineral, anatase, Fe-bearing minerals, goethite and hematite dominating. Gibbsite was present mainly in minor amounts. The formation of gibbsite could be either through neoformation from the weathering of feldspars which are primary minerals in basalt or by progressive dissolution of kaolinite through desilication under intense weathering (Schaefer et al., 2008). The dominance of kaolinite coupled with gibbsite is indicative of high degree of weathering of the soils (Kanket, 2006). The presence of anatase, goethite, and hematite could be attributed to the relative accumulation by weathering of mafic minerals rich in Ti and Fe (Wiriyakitnateekul et al., 2010). The Al and Fe oxide minerals will have great influences on the fertility particularly on P sorption dynamics in the soils (Hart et al., 2003). In addition, they are important in the retention of plant nutrient elements against leaching under high rainfall (Gilkes and Prakongkep, 2016).

The minerals present in clay fractions developed from granite were kaolinite, quartz, plagioclase feldspar, muscovite/illite, chlorite, and actinolite. Kaolinite dominated the clay minerals (>24 wt %) with chlorite present in minor amounts. The non-clay minerals constituted >69 wt % in all the samples. The presence of a greater percentage of weatherable minerals could be associated with low chemical weathering due to low rainfall regime around Matoks area based on the climatic zone (Conradie, 2012). Further dissolution of the associated weatherable minerals will aid the release of nutrient elements to plants (Gilkes and Prakongkep, 2016).

Quartz was the dominant mineral (>27 wt %) followed by kaolinite in clay fractions developed from arkosic sandstone. The non-clay minerals constituted >69 wt % with weatherable minerals like muscovite and microcline present. The prevailing arid climate around Sagole area (Conradie, 2012) could not have allowed intense weathering of the primary minerals to form kaolinite.

The average abundances of kaolinite from this study which ranges between 23 and 75 wt % were lower than the average values obtained for kaolinites in Thai (95 wt %) and Brazillian (85 wt %) soils (Kanket, 2006). This could be attributed to the more advanced soil developmental stage in the latter by leaching and oxidation associated with greater moisture regime (Kheoruenromne and Suddhiprakarn, 1984; Kanket, 2006).

4.1.1. Kaolinite crystallinity and dehydroxylation temperature

X-ray diffraction-based determination of soil kaolinite crystallinity cannot be successfully used in studying these soil kaolinites since almost pure kaolin samples with little or no impurities is required for such an exercise (Hughes et al., 2009). Hence, the IR spectroscopy-based approach was applied in determining the soil kaolinite crystallinity.

Characteristic bands at 3691-89, 3669, 3651, and 3619 were observed in the studied soil kaolinites in MAT1 0–20 cm, MAT2 0–20 cm, and SA1 0–20 cm, respectively (Table 3a). The IR spectra of soil kaolinites developed from basalt and granite (MAT1 20–50 cm and MAT2 20–50 cm) showed very weak or no inflexion at the bands typical of kaolins. These observations according to the IR empirical (IR-E) approach (Madejova et al., 1997; Vaculikova et al., 2011) which relies on the presence of the kaolinite stretching bands (3691/3689, 3669, 3651/3650, and 3619), the soil kaolinites can possibly be grouped into two classes; partially ordered and poorly ordered. The first class is represented by some soil kaolinites developed from granite and arkosic sandstone which are MAT1 0–20 cm, MAT2 0–20 cm, and SA1 0–20 cm, respectively. The IR spectra of those developed from basalt and granite (MAT1 20–50 cm) belong to the second class because of the absence of the typical kaolin bands.

The IR numerical (IR-N) approach for the soil kaolinites correspond to partially ordered structures based on the IR-N classification (Table 3b). The IR-N classification corresponds well with the first class from IR-E. However, the discrepancy between IR-N and the second class of IR-E could be due to Fe^{3+} substituting for Al in the octahedral sheet of the

Table 5a. Trace elements concentrations (ppm) and average accumulation factors (AFs) of clay fractions developed from different Parent rocks in Limpopo Province, South Africa and for average Thailand Oxisols (basalt) and Ultisols (granite).

Parent Rock	Sample ID	Sc	V	Cr	Co	Ni	Cu	Zn	Rb	Sr	Zr	Ba	Pb	Th	U
Basalt	S1 0–20 cm	43.52	329.95	209.30	32.60	133.30	235.45	79.40	35.08	15.40	208.70	112.75	9.68	4.34	1.17
	S1 20–50 cm	41.36	291.90	191.30	27.67	113.70	239.45	76.05	37.41	10.13	187.65	82.45	9.06	3.97	1.09
	S1 50–100 cm	47.70	384.00	240.60	29.40	159.45	265.45	69.90	4.04	8.13	254.35	61.90	10.77	5.59	1.36
	S2 0–20 cm	38.31	323.50	361.20	27.84	127.95	275.00	74.65	13.64	14.12	175.60	112.10	13.57	3.66	1.00
	S2 20–50 cm	40.28	335.45	398.60	24.29	135.35	300.10	67.35	11.80	9.99	166.45	98.20	7.31	3.60	1.03
	S2 50–100 cm	39.25	248.55	226.00	16.58	123.70	244.50	68.50	7.145	7.53	155.35	69.90	6.50	2.92	0.93
	Average	41.73	318.84	271.17	26.40	132.24	259.99	72.64	18.18	10.88	191.35	84.55	9.48	4.01	1.10
	Average AF	-	-	1.03	0.48	1.11	1.02	0.88	-	-	-	-	0.93	-	-
Granite	MAT1 0–20 cm	8.84	42.34	177.05	6.65	58.20	26.50	48.85	69.05	413.70	1185.60	976.00	23.22	11.10	2.37
	MAT1 20–50 cm	8.67	43.75	178.10	6.97	59.85	29.75	50.90	70.85	372.60	1049.10	943.00	22.17	10.40	2.36
	MAT2 0–20 cm	11.54	59.56	229.90	10.49	92.55	35.70	53.50	81.30	388.10	1285.80	998.50	23.93	12.50	2.79
	MAT2 20–50 cm	10.21	50.05	205.55	7.17	69.60	23.95	44.90	77.10	431.50	1424.50	1127.50	22.57	14.50	3.02
	Average	9.81	48.92	205.55	7.82	70.05	28.98	49.54	74.58	401.46	1236.24	1011.25	22.97	12.15	2.63
	Average AF	-	-	2.54	1.99	2.37	2.17	2.30	-	-	-	-	1.24	-	-
Ark. Sst.	SA1 0–20 cm	12.86	110.85	437.00	8.925	70.10	29.65	53.05	159.30	160.60	1148.3	1220.00	39.59	29.00	5.04
	SA2 0–20 cm	15.52	110.30	351.45	12.19	104.65	53.65	86.00	138.90	147.00	835.15	983.50	31.98	22.90	4.19
	SA2 20–50 cm	15.78	106.25	350.60	12.55	90.90	40.05	82.80	144.30	146.20	733.05	1002.00	32.78	22.20	4.18
	Average	14.72	109.13	379.68	11.22	88.55	41.12	73.95	147.47	151.23	905.50	1068.50	34.78	24.72	4.47
	Average AF	-	-	3.23	1.84	2.23	2.01	-	-	-	-	-	1.71	-	-
Thailand Oxisols[1]	Average	25.00	155.00	124.00	36.00	189.00	58.00	105.00	22.00	322.00	3.00	515.00	11.00	14.00	0.83
Thailand Ultisols[1]	Average	7.20	33.00	36.00	1.90	6.30	14.00	40.00	40.00	6.00	1.70	30.00	17.00	33.00	-

[1] Darunsontaya et al. (2010).

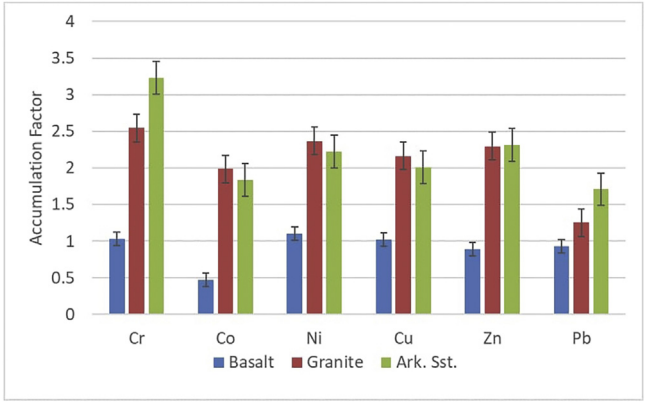

Figure 3. Average accumulation factors in the clay fractions from basalt, granite and arkosic sandstone.

kaolinite structure which could cause lower crystallinity value (Russell and Fraser, 1994; Vaculikova et al., 2011; Oyebanjo et al., 2018).

The dehydroxylation temperature (DT) ranging from 457 to 475 °C and 425 to 467 °C for the soil kaolinites developed from basalt and granite (Table 3b) were lower when compared to the averages for kaolinites in Thai soils (497 °C), Brazillian soils (510 °C) (Melo et al., 2001), West Australian soils (489 °C) (Singh and Gilkes, 1992), reference kaolinite (520–544 °C) (Hart et al., 2002). The presence of Fe and small crystal size has been identified as a cause for the decrease in DT which invariably induces structural disorder (Singh and Gilkes, 1992; Hart et al., 2002).

4.2. Geochemical characteristics

4.2.1. Major oxides

The average values and ranges of the major oxide concentrations are given in Table 4. The clay fractions in soils developed from basalt have higher Al_2O_3 (24.57 wt %) and lower SiO_2 (35.66 wt %) and SiO_2/Al_2O_3 ratio (1.45) mean values relative to those obtained developed from granite and arkosic sandstone (Table 4). This is harmonious with the mineralogy, since the clay fractions in soils developed from basalt have more kaolinite than the other clay fractions in soils developed from granite and arkosic sandstone. LOI was highest in clay fractions in soils developed from basalt. This could be attributed to the higher percentages of kaolinite, goethite, and gibbsite with chemically bound water in their matrices (Beuria et al., 2017). The mean SiO_2/Al_2O_3 ratios for the clay fractions were greater than the value of 1.38 for Thailand Ultisols and 1.16 for Brazillian Ultisols (Table 4).

The variation in the SiO_2/Al_2O_3 ratios suggest different degree of weathering. Soils with lower ratios have experienced higher degree of weathering relative to those with higher ratios (Schaefer et al., 2008). This is consistent with the earlier observations from the mineralogy of the clay fractions.

The TiO_2 and Fe_2O_3 were present in all the clay fractions but highest in those developed from basalt (Table 4). This reflects the mafic nature of basalt with more ferromagnesian minerals (Baioumy, 2014). In addition, Fe_2O_3 mean values for clay fractions developed from basalt and granite were comparable to those obtained for Thailand oxisols and ultisols, respectively (Table 4).

The lowest levels of CaO, MgO, K_2O, and Na_2O were obtained for clay fractions developed from basalts with lower percentages of weatherable minerals relative to other clay fractions. In addition to differences in the rainfall regimes in the study areas earlier mentioned, the observation also reflects the stability of the minerals to alteration. As such, minerals in basalt with higher crystallisation temperatures alter faster to more stable secondary minerals relative to minerals in granite and arkosic sandstone with lower crystallisation temperatures (Naqvi, 2013; Ibarra et al., 2016).

4.2.2. Trace elements

The average values and ranges of trace elements in the clay fractions are presented in Table 5a. The clay fractions developed from basalt contain higher amounts of Sc, V, Co, Ni, and Cu whereas, clay fractions developed from granite have higher concentrations of Zr. Clay fractions from arkosic sandstone derived soils contain higher concentrations of Cr, Rb, Ba, Pb, Th, and U.

Table 5b. Non-carcinogenic hazard index (HI) based on the average trace element concentrations in clay fractions (0–20 cm) developed from different Parent rocks in Limpopo Province, South Africa.

	Basalt				Granite				Ark Sst			
	HQ ing	HQ derm	HQ inh	HI	HQ ing	HQ derm	HQ inh	HI	HQ ing	HQ derm	HQ inh	HI
Children												
Cr	1.14E+00	1.60E-01	8.61E-03	1.31E+00	8.13E-01	1.14E-01	6.14E-03	9.33E-01	1.58E+00	2.21E-01	1.19E-02	1.81E+00
Ni	7.83E-02	8.12E-04	1.25E-03	8.04E-02	4.52E-02	4.68E-04	7.22E-04	4.64E-02	5.24E-02	5.43E-04	8.37E-04	5.37E-02
Zn	2.90E-03	4.06E-05	2.09E-07	2.94E-03	1.98E-03	2.77E-05	1.42E-07	2.01E-03	2.78E-03	3.89E-05	2.00E-07	2.82E-03
Pb	3.98E-02	7.43E-04	2.85E-06	4.06E-02	8.07E-02	1.51E-03	5.77E-06	8.22E-02	1.23E-01	2.29E-03	8.77E-06	1.25E-01
Co	7.97E-04	-	-	7.97E-04	1.61E-03	-	-	1.61E-03	2.45E-03	-	-	2.45E-03
Cu	8.25E-02	7.14E-05	5.50E-06	8.25E-02	1.00E-02	8.70E-06	6.70E-07	1.01E-02	1.35E-02	1.16E-05	8.98E-07	1.35E-02
Total	1.35E+00	1.61E-01	9.87E-03	1.52E+00	9.53E-01	1.16E-01	6.86E-03	1.08E+00	1.77E+00	2.24E-01	1.28E-02	2.01E+00
Adult												
Cr	1.30E-01	2.60E-02	1.97E-03	1.58E-01	9.29E-02	1.85E-02	1.40E-03	1.13E-01	1.80E-01	3.60E-02	2.72E-03	2.19E-01
Ni	9.06E-03	1.34E-04	2.90E-04	9.48E-03	5.16E-03	7.63E-05	1.65E-04	5.40E-03	5.98E-03	8.84E-05	1.91E-04	6.26E-03
Zn	3.32E-04	6.62E-06	4.77E-08	3.38E-04	2.26E-04	4.51E-06	3.25E-08	2.31E-04	3.17E-04	6.33E-06	4.57E-08	3.24E-04
Pb	4.55E-03	1.21E-04	6.51E-07	4.67E-03	8.99E-03	2.39E-04	1.29E-06	9.23E-03	1.40E-02	3.73E-04	2.00E-06	1.44E-02
Co	2.07E-03	-	-	2.07E-03	5.87E-04	-	-	5.87E-04	7.23E-04	-	-	7.23E-04
Cu	9.42E-03	1.16E-05	1.26E-06	9.44E-03	1.15E-03	1.42E-06	1.53E-07	1.15E-03	1.54E-03	1.90E-06	2.05E-07	1.54E-03
Total	1.56E-01	2.63E-02	2.26E-03	1.84E-01	1.09E-01	1.89E-02	1.57E-03	1.29E-01	2.03E-01	3.65E-02	2.92E-03	2.42E-01

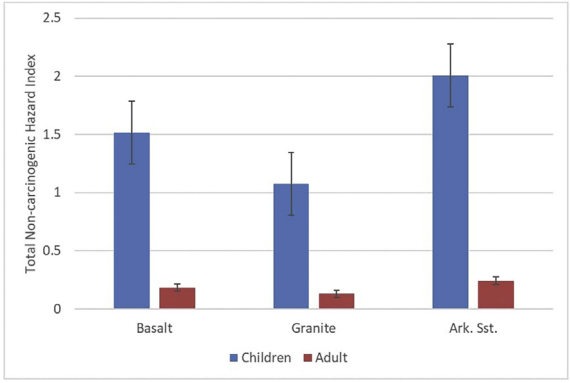

Figure 4a. Average non-carcinogenic hazard indices (HIs) in the clay fractions (0–20 cm) from basalt, granite and arkosic sandstone.

The clay fractions developed from basalt were enriched in Sc, V, Cr, Cu, and Zr, respectively, relative to Thailand oxisols whereas, those developed from granite were enriched in all the trace elements compared to Thailand Ultisols except for Th (Table 5a). This could be attributed to the presence of other weatherable and accessory minerals in the clay fractions from this study. The retention of appreciable proportions of trace elements in the clay fractions has significant implications for soil fertility and geochemical exploration (Kanket et al., 2005).

The average AF values for selected trace elements in the respective parent rocks are presented Table 5a and Figure 3. The trace elements generally show preferential enrichment in the clay fractions (except for Co, Zn, and Pb for clay fractions in soils developed from basalt) relative to the bulk soils.

Higher adsorption capacity in the clay fraction (finer fraction) due to greater surface area per unit of mass have been reported to have caused the preferential partitioning (Wong et al., 2006; Luo et al., 2011; Gomes et al., 2016). Lower AF average values obtained for clay fractions in soils developed from basalt relative to those developed from granite and arkosic sandstone could be due to the presence of lower percentage of weatherable minerals in them (Acosta et al., 2011). Trace element accumulation sequences in the clay fractions were Ni > Cr ≈ Cu > Pb > Zn > Co, Cr > Ni ≈ Zn > Cu > Co > Pb, and Cr > Zn > Ni > Cu > Co > Pb for those developed from basalt, granite, and arkosic sandstone respectively.

The average non-carcinogenic HI for children and adults are presented in Table 5b and Figure 4a. Ingestion pathway was the main means to exposure to the trace elements for both children and adults. The average HQ contributions through oral ingestion accounted for between 88.20 to 88.70 % and 83.80–84.50 % to the total average HI for children and adults, respectively in the clay fractions from basalt, granite, and

Table 5c. Total carcinogenic risk index (TCRI) based on the average trace element concentrations in clay fractions (0–20 cm) developed from different Parent rocks in Limpopo Province, South Africa.

	Basalt			Granite			Ark. Sst.		
	CRI ing	CRI inh	TCRI	CRI ing	CRI inh	TCRI	CRI ing	CRI inh	TCRI
Children									
Cr	4.89E-02	3.10E-02	7.99E-02	3.48E-02	2.21E-02	5.69E-02	6.77E-02	4.29E-02	1.11E-01
Ni	-	9.01E-05	9.01E-05	-	5.20E-05	5.20E-05	-	6.03E-05	6.03E-05
Pb	2.90E-05	-	2.90E-05	5.88E-05	-	5.88E-05	8.93E-05	-	8.93E-05
Total	4.89E-02	3.11E-02	8.00E-02	3.49E-02	2.21E-02	5.70E-02	6.78E-02	4.30E-02	1.11E-01
Adult									
Cr	2.79E-02	3.54E-02	6.34E-02	1.99E-02	2.52E-02	4.52E-02	3.87E-02	4.90E-02	8.77E-02
Ni	-	1.03E-04	1.03E-04	-	5.94E-05	5.94E-05	-	6.89E-05	6.89E-05
Pb	1.66E-05	-	1.66E-05	3.36E-05	-	3.36E-05	5.10E-05	-	5.10E-05
Total	2.80E-02	3.55E-02	6.35E-02	1.99E-02	2.53E-02	4.52E-02	3.87E-02	4.91E-02	8.78E-02

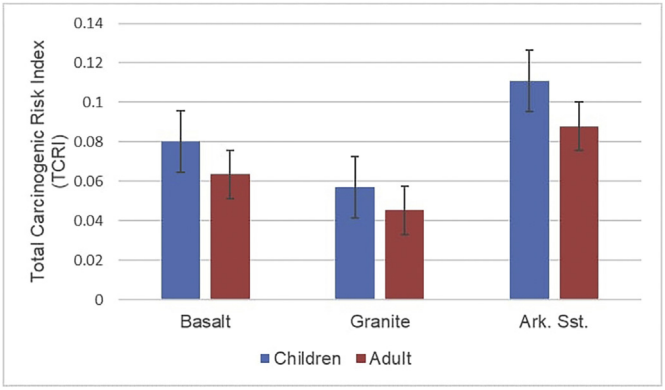

Figure 4b. Average total carcinogenic risk indices (TCRIs) in the clay fractions (0–20 cm) from basalt, granite and arkosic sandstone.

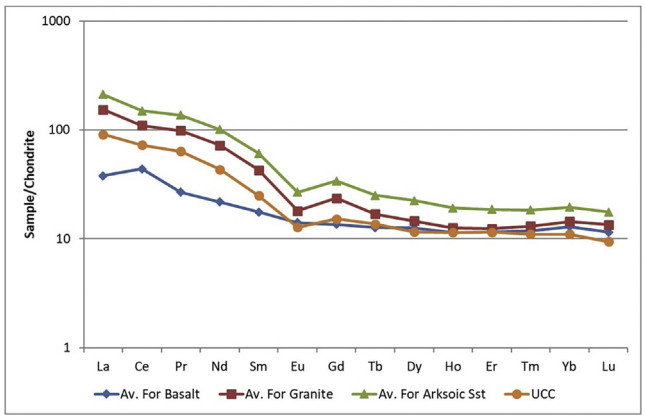

Figure 5. Chondrite-normalised REE pattern of average of the clay fractions developed from different Parent rocks in Limpopo Province, South Africa and for average UCC.

arkosic sandstone. The average HQ values for the trace elements were generally <1 (children and adults) except for Cr in children exposed to clay fractions from basalt and arkosic sandstone (Table 5b).

The adults average non-carcinogenic HI (<1) was lower relative to children (HI > 1, except for clay fractions from granite with HI ≈ 1) for all the clay fractions (Figure 4a). HI > 1 for children indicated that they are susceptible to suffer non-carcinogenic health risk when exposed to the clay fractions. The non-carcinogenic risk for children and adults was clay fractions from arkosic sandstone > basalt > granite, respectively.

The CRI based on the presence of Cr, Ni, and Pb in the clay fractions are presented in Table 5c and Figure 4b. The average CRI due to ingestion pathway was higher than the inhalation route for children but it is the opposite for adults with inhalation route higher than ingestion pathway. This suggest that the main exposure routes for the children and adults were oral ingestion and inhalation, respectively. In this study, Cr contributed more than the other trace elements through the various pathways. The average CRI values in children and adults were generally $>10^{-3}$. This is not within the $10^{-6} < CRI < 10^{-4}$ tolerable limit and suggests very high carcinogenic risk to both children and adult population (USEPA, 2012; Chen et al., 2016; Weissmannová et al., 2019). The decreasing order of CR for children and adults was clay fractions from arkosic sandstone > basalt > granite (Figure 4b). Efficient and inexpensive soil remediation strategies will be required. Sharma et al. (2018) and Kumar et al. (2019) advocated for phytoremediation in addition to traditional remediation strategies to remove contaminants from agricultural soils.

4.2.3. *Rare earth elements (REEs)*

The REE abundances in the clay fractions are listed in Table 6. The absolute mean LREE and HREE concentrations were in order of clay fractions developed from arkosic sandstone > granite > basalt. The average UCC generally showed relative depletion in the REEs in comparison to the average clay fractions developed from basalt, granite, and arkosic sandstone.

However, average REEs obtained for UCC were enriched relative to clay fractions developed from basalt (Table 6). When the average REE contents of the clay fractions and UCC were normalised to chondrite values (Haskin et al., 1971) (Figure 5), clay fractions developed from arkosic sandstone and granite showed pronounced Eu anomalies whereas, those developed from basalt lack distinct Eu anomaly. However, they all showed a general trend of REE fractionation with the enrichment of LREE relative to HREE. The absence of negative Ce anomaly in the trends suggest that the alteration of the primary

Table 6. REE concentrations (ppm) of clay fractions developed from different Parent rocks in Limpopo Province, South Africa and for average Upper Continental Crust (UCC).

Parent Rock	Sample ID	La	Ce	Pr	Nd	Sm	Eu	Gd	Tb	Dy	Ho	Er	Tm	Yb	Lu
Basalt	S1 0–20 cm	16.74	39.46	4.01	17.25	4.32	1.26	4.34	0.76	4.83	0.97	2.71	0.42	2.89	0.41
	S1 20–50 cm	12.18	37.43	2.73	12.14	2.80	0.90	3.06	0.58	3.53	0.77	2.18	0.33	2.29	0.36
	S1 50–100 cm	15.01	55.16	3.74	16.16	4.41	1.18	4.01	0.67	4.78	0.96	2.87	0.43	3.11	0.46
	S2 0–20 cm	9.75	26.60	2.23	10.30	2.47	0.73	2.76	0.54	3.05	0.68	1.93	0.29	2.26	0.35
	S2 20–50 cm	7.69	22.47	1.78	7.90	1.75	0.67	2.15	0.38	2.54	0.55	1.77	0.26	1.94	0.29
	S2 50–100 cm	6.12	23.29	1.39	6.08	1.33	0.44	1.63	0.30	2.05	0.48	1.44	0.24	1.74	0.26
	Average	11.25	34.06	2.64	11.64	2.84	0.86	2.99	0.54	3.46	0.74	2.15	0.33	2.37	0.36
Granite	MAT1 0–20 cm	47.39	89.83	10.09	39.85	7.07	1.04	5.37	0.73	4.10	0.78	2.10	0.35	2.71	0.41
	MAT1 20–50 cm	44.82	84.16	9.58	37.95	6.56	1.10	5.11	0.70	3.62	0.72	2.13	0.32	2.37	0.42
	MAT2 0–20 cm	61.09	120.35	13.27	52.15	9.61	1.67	6.98	0.98	5.39	1.12	3.01	0.45	3.17	0.56
	MAT2 20–50 cm	56.78	106.60	12.56	49.50	8.60	1.46	7.02	0.88	5.03	1.01	2.91	0.50	3.50	0.52
	Average	52.52	100.24	11.37	44.86	7.96	1.32	6.12	0.82	4.53	0.91	2.53	0.41	2.94	0.48
Ark. Sst.	SA1 0–20 cm	76.25	146.15	16.32	64.00	11.62	1.73	8.82	1.24	7.31	1.42	4.06	0.64	4.42	0.66
	SA2 0–20 cm	67.29	125.97	14.70	59.15	10.65	1.92	8.14	1.15	6.69	1.26	3.63	0.52	3.69	0.59
	SA2 20–50 cm	65.74	123.53	14.78	57.80	10.85	1.89	8.34	1.14	6.37	1.35	3.50	0.48	3.62	0.55
	Average	69.76	131.88	15.27	60.32	11.04	1.84	8.43	1.18	6.79	1.34	3.73	0.55	3.91	0.60
UCC[1]	Average	30	64	7.1	26	4.5	0.9	3.8	0.64	3.5	0.8	2.3	0.33	2.2	0.3

[1] McLennan (2001).

minerals in the parent rocks took place under suboxic conditions since minerals formed in equilibrium with oxic marine waters are likely to show a negative Ce anomaly (Jeans et al., 2000; Arslan et al., 2006).

5. Conclusion

The study revealed that the dominant clay mineral in the clay fractions was kaolinite with highest percentage in clay fractions developed from basalt. Other minerals present were quartz, plagioclase, microcline, muscovite/illite, anatase, goethite, hematite, gibbsite, chlorite, and actinolite. The percentage of weatherable minerals present in clay fractions were in those developed from granite and arkosic sandstone which accounted for the greater amounts of CaO, MgO, K_2O, and Na_2O relative to clay fractions developed from basalt. The interaction between parent rock influence, climate, and intensity of weathering played a major role in explaining the variations in the mineralogy and geochemistry of the clay fractions of the soils in the study area. The crystallinity based on FTIR showed that the soil kaolinites were partially to poorly ordered. The dehydroxylation temperatures ranged from 425 – 475 °C for the soil kaolinites. The presence of some trace elements in the clay fractions have significant health implications with more enrichments relative to the bulk (except for Co, Zn, and Pb for clay fractions in soils developed from basalt). The children population may be more susceptible to non-carcinogenic health risk relative to the adults whereas, both the children and adults are posed with carcinogenic health risk through ingestion pathway for children and inhalation pathway for adults. The health risk assessment further indicated that Cr is the main contaminant in the clay fractions. Hence, efficient mitigation strategies to remediate the soils are necessary.

Declarations

Author contribution statement

O. O. Oyebanjo: Conceived and designed the experiments; Performed the experiments; Analyzed and interpreted the data; Contributed reagents, materials, analysis tools or data; Wrote the paper.

G. E. Ekosse: Performed the experiments; Contributed reagents, materials, analysis tools or data.

J. O. Odiyo: Contributed reagents, materials, analysis tools or data.

Funding statement

O. Oyebanjo was supported by the University of Venda (S999). G. E. Ekosse was supported by the National Research Foundation (ZA) (CPRR UID 91559).

Data availability statement

Data associated with this study has been deposited at UNIVERSITY OF VENDA LIBRARY https://univendspace.univen.ac.za/handle/11602/1519.

Declaration of interests statement

The authors declare no conflict of interest.

Additional information

No additional information is available for this paper.

References

Acosta, J.A., Cano, A.F., Arocena, J.M., Debela, F., Martínez-Martínez, S., 2009. Distribution of metals in soil particle size fractions and its implication to risk assessment of playgrounds in Murcia City (Spain). Geoderma 149, 101–109.

Acosta, J.A., Faz, A., Kalbitz, K., Jansen, B., Martinez-Martinez, S., 2011. Heavy metal concentrations in particle size fractions from street dust of Murcia (Spain) as the basis for risk assessment. J. Environ. Monit. 13, 3087–3096.

Ajmone-Marsan, F., Biasioli, M., Kralj, T., Grcman, H., Davidson, C.M., Hursthouse, A.S., Madrid, L., Rodrigues, S., 2008. Metals in particle-size fractions of the soils of five European cities. Environ. Pollut. 152, 73–81.

Arslan, M., Kadir, S., Abdioglu, E., Kolayli, H., 2006. Origin and formation of kaolin minerals in saprolite of Tertiary alkaline volcanic rocks, Eastern Pontides, NE Turkey. Clay Miner. 41, 597–617.

Baioumy, H.M., 2014. Geochemistry and origin of the Cretaceous sedimentary kaolin deposits, Red Sea, Egypt. Chem. Erde 74, 195–203.

Barker, O.B., Brandl, G., Callaghan, C.C., Eriksson, P.G., Van der Neut, M., 2006. The Soutpansberg and waterberg groups and the blouberg formation. In: Johnson, M.R., Anhaeusser, C.R., Thomas, R.J. (Eds.), The Geology of South Africa: Johannesburg. Geological Society of South Africa and Pretoria, Council for Geoscience, pp. 301–318.

Barton Jr., J.M., Doig, R., Smith, C.B., Bohlender, F., Van Reenen, D.D., 1992. Isotopic and REE characteristics of the intrusive charnoenderbite and enderbite geographically associated with the Matok Pluton, Limpopo Belt, southern Africa. Precambrian Res. 55, 451–467.

Beuria, P.C., Biswal, S.K., Mishra, B.K., Roy, G.G., 2017. Study on kinetics of thermal decomposition of low LOI goethetic hematite iron ore. Int. J. Min. Sci. Technol. 27 (6), 1031–1036.

Brandl, G., 1981. The geology of the Messina area. Explan. Sheet 2230 (Messina). Geol. Surv. S. Afr., pp. 1–35

Brandl, G., 1999. Soutpansberg Group. In: Johnson, M.R. (Ed.), Catalogue of South African Lithostratigraphic Unit. S. Afr. Comm. Strat., pp. 6–39–6–41

Chen, H., Teng, Y., Lu, S., Wang, Y., Wu, J., Wang, J., 2016. Source apportionment and health risk assessment of trace metals in surface soils of Beijing metropolitan, China. Chemosphere 144, 1002–1011.

Cheney, E.S., Barton, J.M., Brandl, G., 1990. Extent and age of the Soutpansberg sequence of South Africa. S. Afr. J. Geol. 93 (4), 664–675.

Conradie, D.C.U., 2012. South Africa's climatic zones: today, tomorrow. In: Paper Presented at the International Green Building Conference and Exhibition, Sandton, South Africa, p. 9.

Darunsontaya, T., Suddhiprakarn, A., Kheoruenromne, I., Gilkes, R.J., 2010. Geochemical properties and the nature of kaolin and iron oxides in upland oxisols and ultisols under a tropical monsoonal climate, Thailand. Thai J. Agric. Sci. 43, 197–215.

Ekosse, G., 2005. X-ray Powder Diffraction Patterns of Clays and clay Minerals in Botswana. Associated printers, Gaborone, Botswana, p. 78.

Fey, M.V., 2010. A short guide to the soils of South Africa, their distribution and correlation with World Reference Base soil groups. In: 19th World Congress of Soil Science, Soil Solutions for a Changing World, pp. 32–35.

Gao, L., Wang, Z., Zhu, A., Liang, Z., Chen, J., Tang, C., 2019. Quantitative source identification and risk assessment of trace elements in soils from Leizhou Peninsula, South China. Hum. Ecol. Risk Assess. 25 (7), 1832–1852.

Gilkes, R.J., Prakongkep, N., 2016. How the unique properties of soil kaolin affect the fertility of tropical soils. Appl. Clay Sci. 131, 100–106.

Gomes, P., Valente, T., Braga, M.A., Grande, J.A., de la Torre, M.L., 2016. Enrichment of trace elements in the clay size fraction of mining soils. Environ. Sci. Pollut. Res. 23 (7), 6039–6045.

Günther, D., Hattendorf, B., 2005. Solid sample analysis using laser ablation inductively coupled plasma mass spectrometry. Trends Anal. Chem. 24 (3), 255–265.

Hall, R., Wisborg, P., Shirinda, S., Zamchiya, P., 2013. Farm workers and farm dwellers in Limpopo Province, South Africa. J. Agrar. Change 13 (1), 47–70.

Haskin, L.A., Helmke, P.A., Paster, T.P., Allen, R.O.(, 1971. Rare earths in Meteoric, terrestrial, and lunar matter. In: Activation Analysis in Geochemistry and Cosmochemistry.

Hart, R.D., Gilkes, R.J., Siradz, S., Singh, S., 2002. The nature of soil kaolins from Indonesia and Western Australia. Clay Clay Miner. 50, 198–207.

Hart, R.D., Wiriyakitnateekul, W., Gilkes, R.J., 2003. Properties of soil kaolins from Thailand. Clay Miner. 38, 71–94.

Herselman, J.E., 2007. The Concentration of Selected Trace Metals in South African Soils. University of Stellenbosch, South Africa. Unpublished PhD Thesis.

Hillier, S., 2000. Accurate quantitative analysis of clay and other minerals in sandstones by XRD: comparison of a Rietveld and a reference intensity ratio (RIR) method and the importance of sample preparation. Clay Miner. 35, 291–302.

Hughes, J.C., Gilkes, R.J., Hart, R.D., 2009. Intercalation of reference and soil kaolins in relation to physico-chemical and structural properties. Appl. Clay Sci. 45, 24–35.

Ibarra, D., Caves Rugenstein, J., Moon, S., Thomas, D., Hartmann, J., Chamberlain, C., Maher, K., 2016. Differential weathering of basaltic and granitic catchments from concentration-discharge relationships. Geochem. Cosmochim. Acta 190, 265–293.

Jakubowska, J., 2007. Effects of Irrigation Water Type on Soil Organic Matter (SOM) Fractions and Their Interactions with Hydrophobic Compounds. PhD Thesis, Martin-Luther-Universität Halle-Wittenberg, Halle, Germany.

Jeans, C.V., Wray, D.S., Merriman, R.J., Fisher, M.J., 2000. Volcanogenic clays in Jurassic and cretaceous strata of England and the north sea basin. Clay Miner. 35, 25–55.

Kabata-Pendias, A., 2011. Trace Elements in Soils and Plants, fourth ed. CRC Press, Boca Ratón. Florida, p. 505.

Kanket, W., 2006. Properties of the Clay Fraction of Alfisols and Ultisols in Thailand PhD Thesis. Kasetsart University, Bangkok, Thailand.

Kanket, W., Suddhiprakarn, A., Kheoruenromne, I., Gilkes, R.J., 2005. Chemical and crystallographic properties of kaolin from ultisols in Thailand. Clay Clay Miner. 53, 478–489.

Kheoruenromne, I., Suddhiprakarn, A., 1984. Ecology, classification and effect of management of selected sandy soils in Thailand. In: Ecology and Management of Problem Soils in Asia. FFTC Book Series No. 27, Taipei, Taiwan, pp. 207–224.

Kicinska, A., 2018. Health risk assessment related to an effect of sample size fractions: methodological remarks. Stoch. Environ. Res. Risk Assess. 32, 1867–1887.
Kumar, V., Pandita, S., Sharma, A., Bakshi, P., Sharma, P., Karaouzas, L., Bhardwaj, R., Thukral, A.K., Cerda, A., 2019. Ecological and human health risks appraisal of metal(loid)s in agricultural soils: a review. Geol. Ecol. Landsc.
Luo, X.S., Yo, S., Li, X.D., 2011. Distribution, availability, and sources of trace metals in different particle size fractions of urban soils in Hong Kong: implications for assessing the risk to human health. Environ. Pollut. 159, 1317–1326.
Luo, X.S., Ding, J., Xu, B., Wang, Y.J., Li, H.B., Yu, S., 2012. Incorporating bioaccessibility into human risk assessments of heavy metals in urban park soils. Sci. Total Environ. 424, 88–96.
Madejová, J., Kraus, I., Tunega, D., Šamajová, E., 1997. Fourier transform infrared spectroscopic characterization of kaolin group minerals from the main Slovak deposits. Geol. Carph. Ser. Clay 6 (1), 3–10.
Madejová, J., Komadel, P., 2001. Baseline studies of the clay minerals source society: infrared methods. Clay Clay Miner. 49, 410–432.
McLennan, S.M., 2001. Relationships between the trace element composition of sedimentary rocks and upper continental crust. Geochem. Geophys. Geosyst. 2, 1021.
Melo, V.F., Singh, B., Schaefer, C.E.G.R., Novais, R.F., Fontes, M.P.F., 2001. Chemical and mineralogical properties of kaolinite-rich Brazilian soils. Soil Sci. Soc. Am. J. 65, 1324–1333.
Mzezewa, J., Misi, T., van Rensburg, L., 2010. Characterisation of rainfall at a semi-arid ecotope in the Limpopo Province (South Africa) and its implications for sustainable crop production. WaterSA 36 (1), 19–26.
Naqvi, S.A., 2013. Weathering of Precambrian Basement and Formation of Sedimentary Particles in Scania. Unpublished MSc Thesis, University of Oslo, Norway.
Oyebanjo, O.M., Ekosse, G.E., Odiyo, J.O., 2018. Mineral constituents and kaolinite crystallinity of the <2μm fraction of cretaceous-paleogene/neogene kaolins from eastern dahomey and Niger Delta Basins, Nigeria. Open Geosci. 10, 157–166.
Oyebanjo, O.O., Ekosse, G.E., Odiyo, J.O., 2020. Geochemistry of Oxidic Soils Developed from Different Parent Rocks in the Limpopo Province, South Africa. Transactions of the Royal Society of South Africa.
Oyebanjo, O.O., 2020. Mineralogy and Geochemistry of Kaolins in Oxidic Soils Developed from Different Parent Rocks in Limpopo Province, South Africa. University of Venda, South Africa, p. 312.
Qing, X., Yutong, Z., Shenggao, L., 2015. Assessment of heavy metal pollution and human health risk in urban soils of steel industrial city (Anshan), Liaoning, Northeast China. Ecotoxicol. Environ. Saf. 120, 377–385.
Räty, M., Peltovuori, T., 2008. Sorption of phosphate phosphorus in ultrasound-separated particle-size fractions from arable soils. NJF Rep. 4, 147–151.
Robb, L.J., Brandl, G., Anhaeusser, C.R., Poujol, M., 2006. Archaean granitoid intrusions. In: Johnson, M.R., Anhaeusser, C.R., Thomas, R.J. (Eds.), The Geology of South Africa: Johannesburg. Geological Society of South Africa and Pretoria, Council for Geoscience, pp. 57–94.
Russell, J.D., Fraser, A.R., 1994. In: Wilson, M.J. (Ed.), Clay Mineralogy: Spectroscopic and Chemical Determinative Methods. Chapman & Hall, London, UK, p. 11.
Schaefer, C.E., Fabris, J.D., Ker, J.C., 2008. Minerals in the clay fraction of Brazilian Latosols (Oxisols): a review. Clay Miner. 43, 137–154.
Sharma, R., Bhardwaj, R., Gautam, V., Bali, S., Kaur, R., Kaur, P., Ohri, P., 2018. Phytoremediation in waste management: hyperaccumulation diversity and techniques. In: Hasanuzzaman, Mirza, Nahar, Kamrun (Eds.), Fujita, Masayuki: Plants under Metal and Metalloid Stress. Springer.
Singh, B., Gilkes, R.J., 1992. Properties of soil kaolins from south-western Australia. J. Soil Sci. 43, 645–667.
South African Committee for Stratigraphy (SACS), 1980. Stratigraphy of South Africa, Pt. 1. Compiled by L.E. Kent. In: Handbook of the Geological Survey.
SOIL SURVEY STAFF, 2006. Keys to soil taxonomy. In: Suslick, K.S., Price, G.J. (Eds.), (1999). Applications of Ultrasound to Materials Chemistry, , tenth ed.29. USDA-NRCS, Washington DC, pp. 295–326. Annu. Rev. Mater. Sci.
Suslick, K.S., Price, G.J., 1999. Applications of ultrasound to materials Chemistry. Annu. Rev. Mater. Sci. 29, 295–326.
Trakoonyingcharoen, P., Kheoruenromne, I., Suddhiprakarn, A., Gilkes, R.J., 2006. Properties of kaolins in red oxisols and red ultisols in Thailand. Appl. Clay Sci. 32, 25–39.
U.S. Environmental Protection Agency (USEPA, 2012. Integrated Risk Information System of the US Environmental Protection Agency. US Environmental Protection Agency (USEPA), Washington, DC, USA.
Vaculíková, L., Plevová, E., Vallová, S., Koutník, I., 2011. Characterization and differentiation of kaolinites from selected Czech deposits using infrared spectroscopy and differential thermal analysis. Acta Geodyn. Geomater. 8 (1), 59–67 (161).
Van Reeuwijk, L.P., 2002. Procedures for Soil Analysis. International Soil Reference and Information Centre, p. 100. Wageningen, The Netherlands, Tech. Paper 9.
Weissmannová, H.D., Mihočová, S., Chovanec, P., Pavlovský, J., 2019. Potential ecological risk and human health risk assessment of heavy metal pollution in industrial affected soils by coal mining and metallurgy in Ostrava, Czech republic. Int. J. Environ. Res. Publ. Health 16, 1–19.
Wiriyakitnateekul, W., Suddhiprakarn, A., Kheoruenromne, I., Saunders, M., Gilkes, R.J., 2010. Characteristics of soil kaolin on various parent materials in Thailand. In: 19th World Congress of Soil Science, Soil Solutions for a Changing World, pp. 18–21.
Wong, C.S., Li, X.D., Thornton, I., 2006. Urban environmental geochemistry of trace metals. Environ. Pollut. 142, 1–16.
WRB (World Reference Base for Soil Resources), 2006. A framework for international classification, correlation and communication. World Soil Resour. Rep. 103. IUSS/ISRIC/FAO.
Yoothong, K., Moncharoen, L., Vijarnsorn, P., Eswaran, H., 1997. Clay mineralogy of Thai soils. Appl. Clay Sci. 11, 357–371.